Identification of Wood Species by Acoustic-Resonance Spectrometry Using Multivariate Subpopulation Analysis

TIMOTHY P. MILLS, ANGELA JONES, and ROBERT A. LODDER*

Department of Chemistry, University of Kentucky, Lexington, Kentucky 40506-0055 (T.P.M.); and College of Pharmacy, University of Kentucky Medical Center, Lexington, Kentucky 40536-0082 (A.J., R.A.L.)

The identification of wood species remains an issue in restoration involving rare, old, or disguised wood parts. Precise restoration is required in reconditioning the works of designers such as Frank Lloyd Wright, and a quick, reliable, and nondestructive method of identification facilitates this restoration. Acoustic-resonance spectrometry (ARS) is an analytical method using interferences in resonance signals across a range of frequencies. Combined with multivariate analysis techniques, ARS is a solution to the problem of identifying wood species. Subpopulation detection analysis of samples of 26 different wood species achieved complete differentiation among species (p = 0.01). The number of bootstrap replications of the spectral data has a significant effect on differentiation among the woods, as does the type of spectral filtering prior to subpopulation analysis. Acoustic-resonance spectrometry outperforms near-IR spectrometry by a wide margin in identification of the same wood species.

Index Headings: **Acoustic-resonance spectrometry; Bootstrap; Furniture; Historic buildings.**

INTRODUCTION

In 1974 a group of Chicago residents took a historic responsibility when they formed the Frank Lloyd Wright Home and Studio Foundation and purchased the architect's first home built in 1889.[1] In renovating the landmark, the chief consideration was restoring the structure to its original state. This task included extensive research of old records and drawings, and analysis of various building materials to ensure that the same paint, wood, and plaster were used in the refurbishing. In this $2.1 million project, wood species verification was particularly important because Wright consistently utilized native woods in his work. In this instance, with 33 custom-trim profiles cut from various kinds of wood, every wall in all nine rooms needed some trim replacing. Most of these required new sashes and doors. Identifying the type, age, and finish on wood, however, can be a challenging operation in itself because of the variables that combine to give wood its appearance.[2] Many species can be stained to look like other woods and may not be distinguishable until the wood is cut and bled. In the restoration of Wright's home, renovators had to send fragile wood samples, which had become brittle over the years, to a lab for analysis. With the use of acoustic-resonance spectrometry, nondestructive analysis could be conducted on-site, ensuring historically accurate and cost-effective restoration.

With the use of ultrasonic techniques, it has been found that absorption of acoustic energy in wood is linear up to 4 MHz, and that acoustic velocity in wood exhibits directional dependence.[3] Ultrasonic tomography has been employed in the nondestructive testing of internally damaged wooden poles, such as those used for power distribution and communication.[4] The acoustic-resonance spectrometer employed in this paper is inspired by an instrument used in the analysis of small amounts of pure liquids.[5] The present paper combines this new acoustic-resonance spectrometer with a subpopulation detection algorithm to determine the species of wood samples nondestructively.

Subpopulation detection has been shown to be a valuable tool in multivariate spectroscopic analysis where the underlying distribution of the data is unknown.[6] The subpopulation detection technique considers each analytical wavelength to be an independent spatial dimension, and n spectra taken at p wavelengths are represented as n points in a p-dimensional hyperspace. Spectra of similar samples tend to cluster together in the same region of hyperspace. The algorithm differentiates between spectra from two samples in a similar region by comparing the integrals of the spectral distributions from the center of one sample spectral group outward. A confidence limit is set on the correlation between the two sample integrals, and the value of the correlation is used to identify new spectra by comparing test spectra to a library of calibration sample spectra.

Quantile-Q uantile (QQ) plots provide an efficient method of visualizing spectral subpopulation distributions in hyperspace.[7] Correlation coefficients are calculated from QQ plots of the integrals of two probability density functions, which form cumulative distribution functions (CDFs). The CDF of the calibration spectra forms the theoretical cumulative distribution function (TCDF). The TCDF is plotted on the abscissa. The union of the calibration and test spectral sets produces the empirical CDF (ECDF). The ECDF is plotted on the ordinate. If the calibration spectra and the test spectra occupy the same position in p-space and share the same size and shape, the QQ plot will be a straight line with unity slope. When the two distributions are separated in p-space, a break appears in the QQ line, forming two line segments in the QQ plot. The vertical separation between the two line segments on the QQ plot is proportional to the euclidean distance between the calibration spectra and test spectra in p-space. The slope of the line segments is proportional to the scale of the calibration spectral distribution and test spectral distribution in hyperspace. The correlation coefficients are used to assess how well the ECDF matches the TCDF.

THEORY

In general, sound is the transmission of energy via successive compressions and rarefactions of molecules in

Received 1 June 1993.

* Author to whom correspondence should be sent.

0003-7028/93/4711-1880$2.00/0

the transport medium. The compression and expansion process can occur in the direction of propagation (longitudinal) or perpendicular to the direction of propagation (transverse). Complex modes of propagation can be set up in bounded solids in which the velocity of the sound wave is frequency dependent. This complex behavior arises because any displacement in one direction of the solid medium cannot occur without displacements in other directions as well. In liquids and gases, the only known mode of propagation is the longitudinal wave (also known as the P-wave), but in solids this mode is accompanied by transverse (or S) waves. In any case, longidutinal waves travel at almost twice the velocity of the transverse wave.

The acoustic-resonance technique depends in large part on the fact that the velocity of propagation of a sound wave is characteristic of the medium in which the wave travels. As a rule, sound waves travel faster in more rigid media. In the acoustic-resonance technique it is desirable to have both a resonating tube and a reflecting surface (which usually doubles as a sample holder) with relatively high characteristic sound velocities. In the resonance tube a high acoustic velocity is important to minimize loss of sound intensity because acoustic impedance is inversely proportional to the characteristic velocity of sound in the medium according to the equation

$$Z_{ac} = P/(vA) \quad (1)$$

where Z_{ac} is the acoustic impedance, P is the sound pressure (which is proportional to the wave amplitude), v is the velocity of the sound wave, and A is an arbitrary unit of area. In addition, when the resonance tube is mechanically loaded by the analyte, any difference (relative to the blank tube) manifested in the resulting spectrum is at least partially attributable to the delayed recombination (constructively or destructively) of the coupled energy to the original resonance wave. Thus, to determine analytes accurately, the characteristic acoustic velocity of the resonance tube should be very different from that of the coupled analyte. The greater the difference in velocity between the tube and sample, the greater the change in peak height resulting from interference. In the reflecting block or sample holder a relatively high velocity of sound also keeps energy loss to a minimum, and causes the phase shift in the resonant wave to be dominated by the delay of the acoustic energy passing through the slower analyte medium.

When resonances are achieved in the tube in contact with the sample across a range of frequencies, each acoustic-resonance spectrum can be regarded as a representation of the coupling strength of the liquid or solid analyte to the resonance tube. This coupling is related to the specific acoustic impedance of the sample. Thus, there are at least two factors that combine to produce a spectrum for a given analyte: the acoustic absorbance and the acoustic velocity of the analyte at each resonant frequency.

For materials of low molecular weight in the frequency range under study, the effect of acoustic velocity dominates the appearance of the acoustic-resonance spectrum. With the use of the most simple available model for a harmonic oscillator, given by

$$\varepsilon = A*\sin(\omega t + \phi) \quad (2)$$

with a period $T = 2\pi/\omega$, amplitude A, resultant signal ε, and phase angle ϕ at time t, the effect of the velocity shift caused by the analyte upon the acoustic-resonance spectrum can be identified.[8] The acoustic signal, which has passed through the analyte once or twice (depending upon whether it was launched from the tube or from a transducer on the aluminum block beneath the sample), adds to the standing wave on the tube and is effectively a phase-shifted signal of the same frequency as the original wave launched from the transmitting transducer lectured on the tube. The observed result at the receiving transducer is a change in signal amplitude, just as observed with absorbance of the wave by the sample.

Figures 1A and 1B demonstrate two important aspects of the acoustic-resonance technique: first, the net signal change with the analyte change at each frequency is cyclical with respect to the velocity shift; second, at low frequencies the net ARS signal changes due to a given range of velocity shift cycles at a much slower rate than at high frequencies. In Fig. 1A, the delay t in the acoustic signal transmitted through the sample is measured relative to the acoustic signal launched directly into the tube. If changes in the composition of the sample cause the delay to vary between 0 and t in Fig. 1A, the absolute value of the observed signal varies between 1.752 and 2. When the acoustic signal is higher in frequency, as in Fig. 1B (which is 5 times the frequency of Fig. 1A), propagation delays in the interval $[0, t]$ cause the absolute value of the observed signal to vary between 0 and 2. At low frequencies sample-velocity-induced changes in peak height are minor, while at high frequencies sample-velocity-induced phase shift may cause the ARS signal at a given frequency to pass through its maximum and minimum multiple times as the signal delay increases from 0 to t. As a result, formulation of a calibration requires nonlinear methods, and the calibration equation is often not even a function in the traditional sense.

In Fig. 1C, the signal values at the low frequency in Fig. 1A are plotted against the signal values at the higher frequency in Fig. 1B. The resulting pattern resembles the Lissajous functions observed when sine waves are applied to the vertical and horizontal inputs of an oscilloscope. A series of synthetic samples with different time delays on the interval $[0, t]$ are shown superimposed on the curve. In reality, the spectra of samples are usually recorded at a large number of frequencies (typically, 10^2 to 10^4 frequencies). The synthetic spectra for Fig. 1 were prepared at four frequencies (1, 2.5, 5, and 10 times the fundamental frequency shown in Fig. 1A). Fig. 1D shows the spectra at all four frequencies in Fig. 1C after transformation to principal axes. While the model presented by the synthetic spectra is a simple one (ignoring resonance and absorbance effects), it is able to generate a calibration curve of great complexity.

The acoustic-resonance spectrum is multivariate in nature. As the frequency of a wave increases, its wavelength decreases in inverse proportion. As the wavelength approaches the dimensions of the atomic or molecular structure, a wave in the normal sense cannot exist. Therefore, there is a frequency limit imposed upon the transmission of acoustic waves through any sample medium,

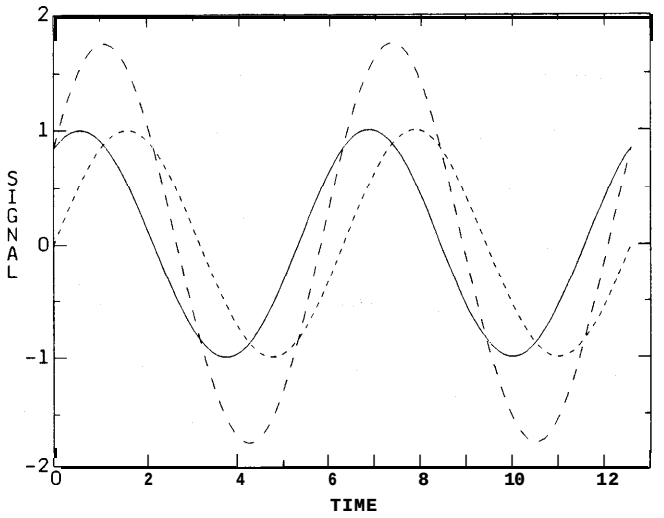

FIG. 1A. The presence of a sample at the vertex of the tube produces a time delay t in the acoustic signal transmitted through the sample relative to the acoustic signal in the tube. For a low frequency, the time delay produces only a minor change in the superposition of the waves observed at the receiving transducer. The solid line represents the signal launched into the tube directly. The dashed line represents the signal launched into the tube through the sample, and the dot-dashed line is the signal observed at the receiving transducer (the time delay in the sample signal is the difference between the solid and dashed lines).

and this limit has been shown to be on the order of MHz for gases and on the order of GHz for liquids and solids. The spectral range covered by the AR spectrometer is well below these limits; thus transmission of the incident waves occurs at all wavelengths. This broad-band transmission means that each spectrum is multivariate in nature, with measurable changes related to the analyte occurring at multiple frequencies.

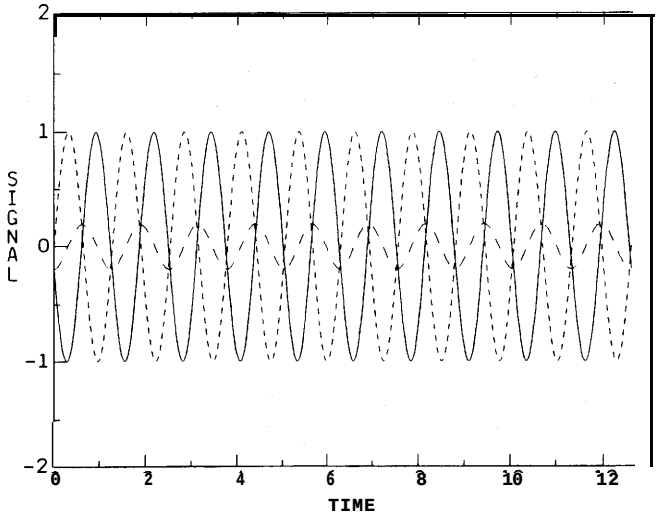

FIG. 1B. At high frequencies (in this example, 5 times the frequency of the fundamental frequency in Fig. 1A), the time delay can be large enough to produce multiple instances of constructive and destructive interference at the receiving transducer. The solid line represents the signal launched into the tube directly. The dashed line represents the signal launched into the tube through the sample, and the dot-dashed line is the signal observed at the receiving transducer.

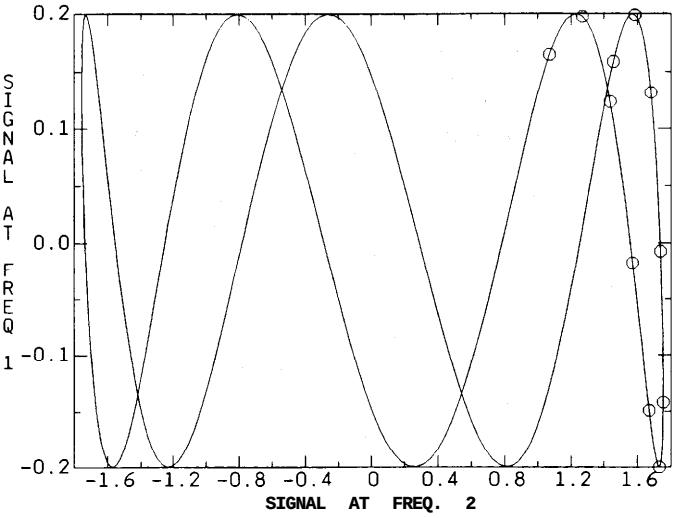

FIG. 1C. Plotting the signals at the frequencies in Figs. 1A and 1B produces a Lissajous curve. The circles on the curve represent spectra of samples with time delays between 0 and t.

EXPERIMENTAL

The spectrometer employed in this experiment was constructed from readily obtainable electronic components. The acoustic excitation signal was generated by an A-D/D-A PC card (Model ML16-P, Industrial Computer Source, San Diego, CA) programmed to send a linear, 7-bit voltage ramp to a voltage-to-frequency converter that generated an electrical signal that varied from 0.5 to 50 kHz. The resulting sine wave was coupled to a polyvinylidene fluoride (PVDF) piezoelectric transmitting transducer that was glued with epoxy to an aluminum coupling plate. The coupling plate in turn was glued to one end of a V-shaped quartz tube with an aluminum bushing. The transducer assembly was shielded electrically inside an aluminum box, and a similar PVDF receiving transducer assembly was positioned on the other

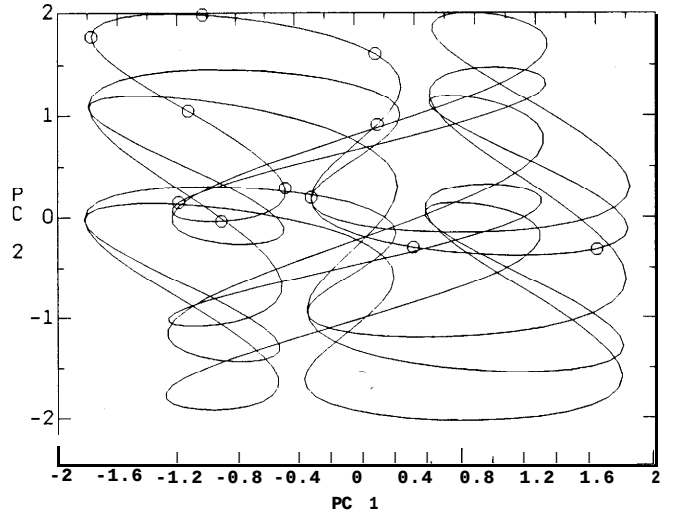

FIG. 1D. Principal-axis transformation of the spectra at all four frequencies (1, 2.5, 5, and 10 times the fundamental frequency) produces a calibration curve of considerable complexity. The circles on the curve represent spectra of the same samples in Fig. 1C.

TABLE I. Wood species used as samples.

1. White ash	14. Maple
2. Beech	15. Maple, bird's eye
3. Birch	16. Oak
4. Cedar	17. Padouk
5. Cherry	18. Pearwood
6. Cypress	19. Rosewood
7. Ebony	20. Satinwood
8. Elm	21. Sycamore
9. Elm, burl	22. Teak
10. Gum	23. Tulip poplar
11. Holly	24. Walnut
12. Mahogany, Honduras	25. Walnut, figured
13. Mahogany, striped	26. Zebrawood

end of the quartz tube. A third transducer assembly was located beneath the sample at the vertex of the tube. Each sample of wood was placed at the vertex of the quartz tube assembly between an aluminum sample holder and the resonance tube. Wood samples were held in place with constant pressure with the use of a spring scale assembly beneath the aluminum sample holder. The signal picked up from the wood by the receiving PVDF transducer was passed through a four-stage operational amplifier, rectified, and coupled to an integrator. The A-D/D-A card read the received signal 100 times at each frequency and recorded the average of the 100 readings. Thirty spectra of each wood sample were obtained at 128 frequencies by reloading the sample at intervals of ten spectra. The wood species examined are listed in Table I. Twenty-six wood wafers approximately 2 cm by 5 cm in size (Schiffer Limited, Exton, PA) were obtained and scanned.

Wood sample spectra were transferred to an IBM 3090-6005 parallel vector supercomputer. Digital filtering and subpopulation detection programs were written in Speakeasy Zeta (Speakeasy Computing Corporation, Chicago, IL). It was hypothesized that the differentiation ability of the acoustic-resonance spectrometer system would improve with the number of bootstrap replications (b) of each calibration and test spectral set. This hypothesis was tested by conducting the analysis of the wood samples with b = 100 and with b = 5000 replications.

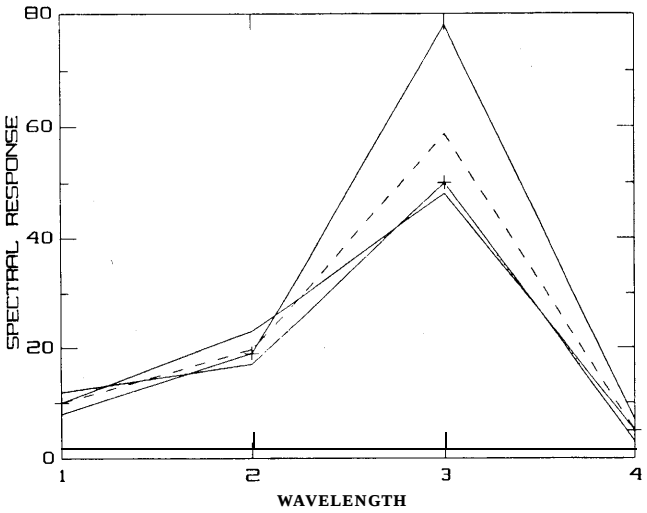

FIG. 3. Each of the three spectral data filters produces a slightly different effect on a hypothetical spectrum. The three raw spectra are depicted with unmarked solid lines, the euclidean-filtered spectrum with the dotted line, the average-filtered spectrum with the dot-dashed line, and the median-values in the spectrum with the plus symbols.

RESULTS AND DISCUSSION

The peaks in an acoustic-resonance spectrum are generated by the resonances of the quartz tube and its associated mechanical parts. The quartz tube resonances are selectively intensified or diminished by interactions with a sample. In general, each sample itself adds no unique peaks to the spectrum, and the variation in resonance intensity at a given wavelength is usually only a

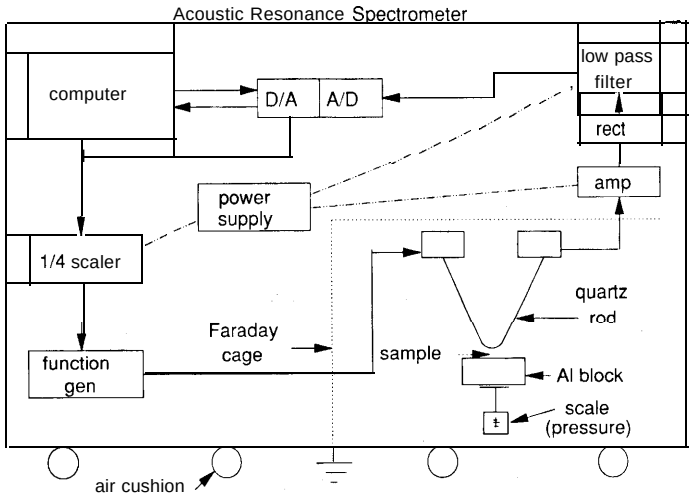

FIG. 2. The diagram of the acoustic-resonance spectrometer. Acoustic waves are launched from the transducer in the box at the top left of the quartz tube, and optionally through the sample at the vertex of the tube. The interference between the waves on the tube and the waves interacting with the sample is monitored at the third transducer located in the box at the top right of the quartz tube.

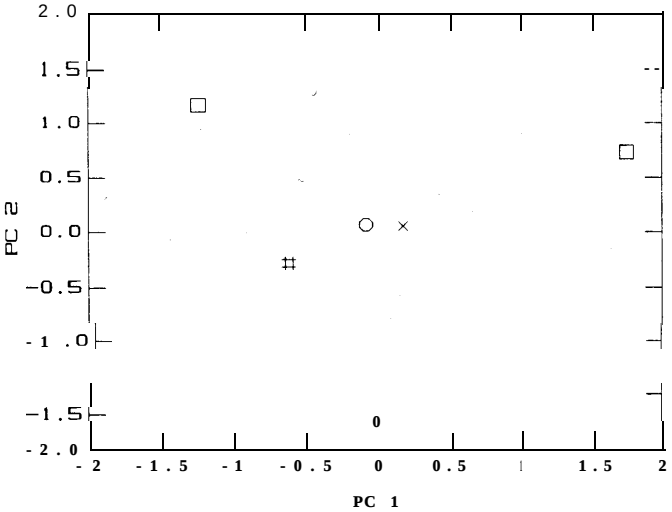

FIG. 4. The spectra from Fig. 3 are translated to principal axes and projected as points in a 2-D space. The three raw spectra are shown as squares, while the euclidean-filtered spectrum appears as a pound symbol, the average-filtered spectrum as an X, and the median-filtered spectrum as an octagon.

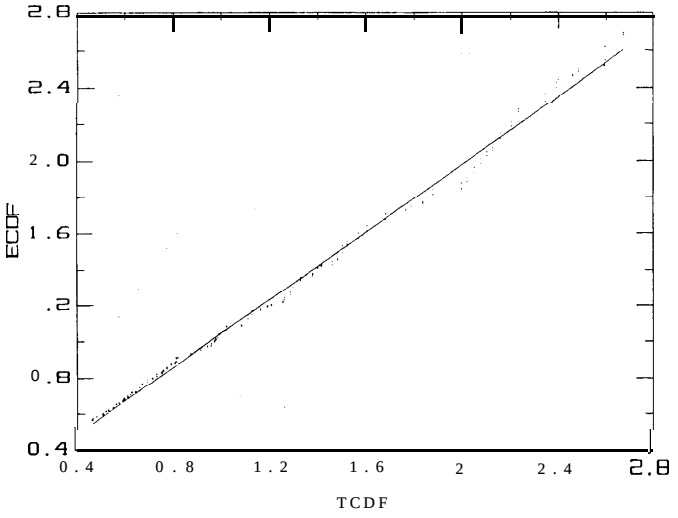

FIG. 5. A QQ plot from odd/even data splitting (training on the odd-numbered wood sample spectra and testing the location and scale of the even-numbered wood spectra) shows no subclustering ($r^2 = 0.99$), suggesting that the woods as a set are similar when all varieties are considered.

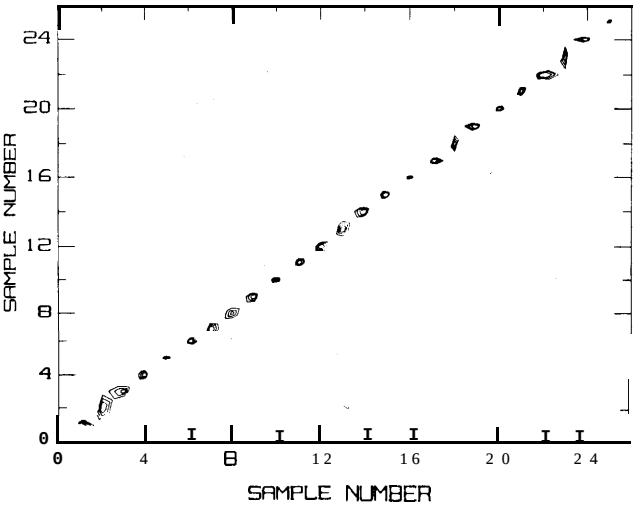

FIG. 7. The ARS spectrometer achieved error-free identification of 26 types of wood with the euclidean filter and 100 bootstrap replications in the subpopulation-detection algorithm. The density contours in this diagram are drawn at distances of up to 3 SDs.

fraction of the resonance peak height (only a portion of the energy from the standing wave is passed from the vertex of the tube through the sample and into the aluminum block). Figure 2 shows the path of acoustic energy transmitted through a sample from the transmitting transducer on the quartz tube and/or the transmitting transducer placed beneath the wood sample.

Quartz was used for the resonance tube because of its high acoustic impedance. In addition, quartz does not act as an antenna for stray rf radiation. In early experiments, the resonances of a solid quartz rod did not couple to the sample as well as those of the hollow tube. Each peak in the acoustic-resonance spectrum represents a resonant condition in the system that cannot be expected to shift in frequency or disappear as long as the dimensions of the system, including the sample, are kept constant (assuming reasonably similar samples are scanned). New resonance peaks do not appear in the spectrum after a change in similar samples (e.g., similarly shaped wood wafers of various species). Therefore, the amplitude of each peak observed in the spectrum at the receiving transducer is a function of the tube resonance and interference between the wave on the quartz tube and the wave passing through the sample over the frequency range being scanned. Both velocity and absorbance of acoustic waves in the sample contribute to the variation in interference.

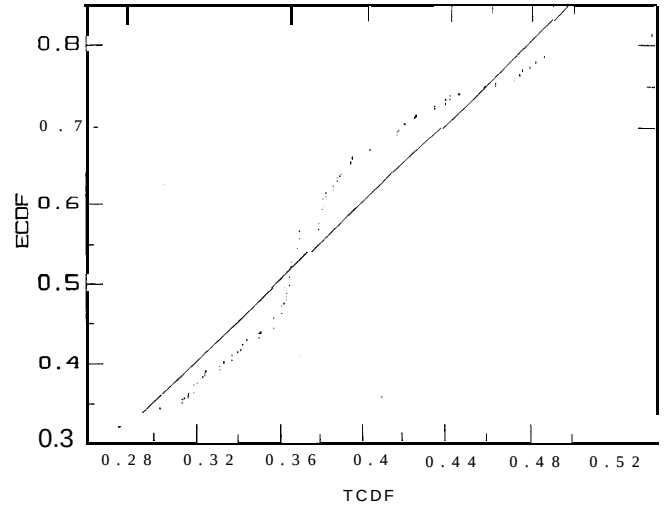

FIG. 6. A QQ plot from first-half/last-half data splitting (training on the first half of the wood sample spectra and testing the location and scale of the second half of the wood spectra) shows no subclustering ($r^2 = 0.98$), suggesting minimal instrumental drift in baseline or gain.

Accurate analysis by ARS requires reproducible spectra from a given sample because acoustic-resonance spectra are not highly specific to particular analytes. A number of measures were taken to reduce noise levels and make spectra more reproducible. The electronics and transducers were shielded in metal boxes, and the entire instrument was enclosed in another metal cabinet that acted as a Faraday cage (a large grounded capacitor). The use of the average of 100 readings on a sample at each frequency to produce each recorded spectral point further reduced noise. In addition, three different data filters were applied to the spectra to test their ability to assist in differentiating among the wood species. The effect of each data filter on a four-frequency segment of hypothetical spectra is depicted in Fig. 3. The same spectra are projected by principal axis transformation as points in 2-D space in Fig. 4. Each of the three filters used three spectra to produce a single spectrum representative of the three. The first filter calculated an average of three spectra, and the second filter calculated a median at each frequency of three spectra. The third filter calculated the euclidean distance in hyperspace between all combinations of three spectra taken two at a time and averaged the values of the two closest spectra.

If the sample acoustic-resonance signal is covered with normal random noise, the average filter is preferable because the noise is reduced the most with this filter. For occasional noise spikes of large amplitude, however, the euclidean or median filter is preferable because the spike is eliminated completely.

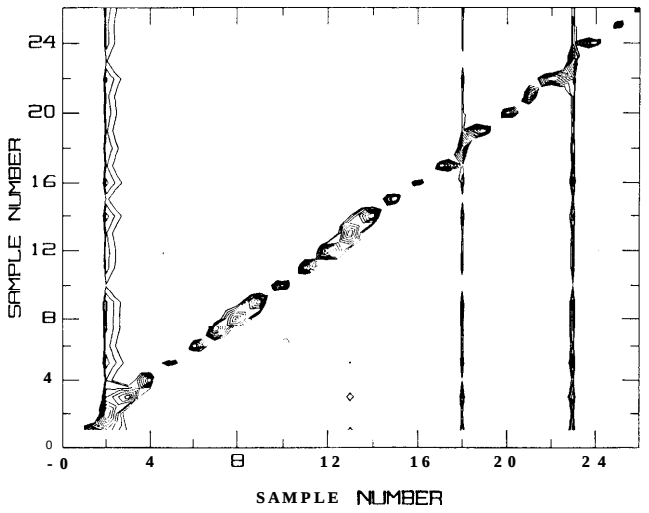

FIG. 8. Extending the density contours in Fig. 7 to distances up to 7 SDs shows that sample numbers 2 (beech), 18 (pearwood), and 23 (tulip poplar) are the most difficult to differentiate from the other samples.

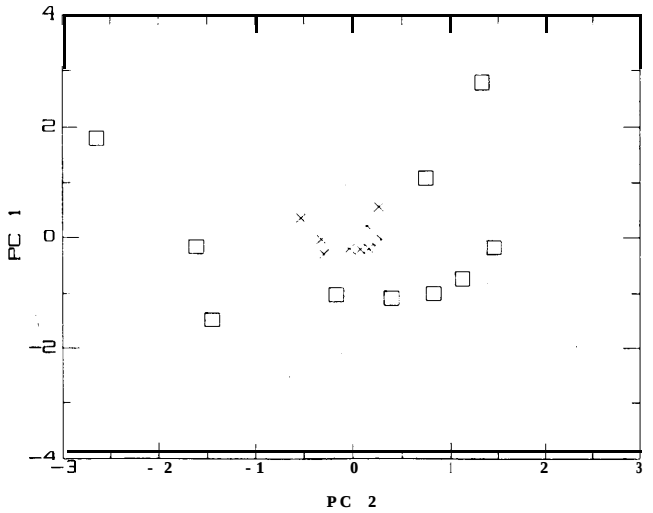

FIG. 9. A principal-component projection of the spectra from one species of wood. The squares mark the original spectra, while the X's mark the same wood spectra after the variation in the spectra is reduced at all wavelengths by a scaling factor.

Figure 5 shows subpopulation cross-validation by odd-even spectral data splitting on the original, unfiltered 30 scans of all samples, with the use of 100 bootstrap replicates in the subpopulation detection algorithm.[6]

Instrumental drift in baseline and gain is minimal over the typical period of each experiment, as demonstrated by data splitting on a first-half/last-half basis (see Fig. 6) of the chronologically ordered raw spectra. Baseline drift was minimized by capacitive coupling of the operational amplifier to the integrator and rectifier. Although a small residual baseline drift could have been corrected in software, such correction was not necessary for subpopulation detection.

A contour plot is an efficient method of illustrating differences between many wood species simultaneously. Changes in location, scale, and skew of the spectral groups from different species are all revealed on contour plots. In order for one to produce a contour plot, the wood species are ordered on both the horizontal and vertical axis, and contour lines are drawn connecting species that are the same number of standard deviations (SDs) apart. The distance in standard deviations between two species is given by

$$(\mu_t - r)/\sigma_t \qquad (3)$$

where μ_t is the mean correlation coefficient between repeated bootstrap replicates of the calibration set; r is the correlation between the integral of the calibration set and the integral of the test set augmented by the calibration set; and σ_t is the standard deviation of the correlation coefficients from repeated bootstrap replications of the calibration set. Thus, a contour plot showing complete differentiation at the level of significance assigned should show no contours except on the diagonal, which compares the end set of spectra to itself.

The performance of the experimental spectral data filters was, from best to worst, euclidean, median, and average. Performance in this case is gauged as the number of samples identified correctly by Eq. 3 and the contour plot. Figure 4 demonstrates that the euclidean filter tends to "tighten" the spectral cluster-an important feature when the distance of separation is dependent on the standard deviation of the distribution. Because of this tightening feature, the contour plots in Figs. 7 and 8 were created with the euclidean spectral filter. Perfect, reproducible separation was achieved at 3 SDs with the use of the euclidean filter and 100 bootstrap replications.

The plots in Figs. 7 and 8 were not highly reproducible at the 7 SD level and showed some contours at different places for each experimental run of the subpopulation detection software. Increasing the number of bootstrap replications to 5000 revealed two points: (1) near-perfect and reproducible separation could be achieved, but achieving it took a great amount of computational time, and (2) interchanging test and training sets had little effect on distances in SDs between samples. As more bootstrap samples were drawn, the bootstrap sample dis-

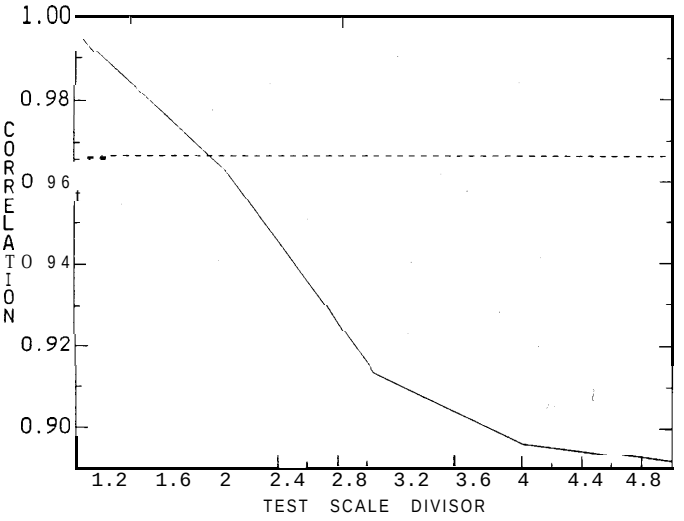

FIG. 10. The effect of the scaling factor on the correlation coefficient from the subpopulation detection algorithm as the test spectral set (the X's in Fig. 9) becomes progressively smaller than the calibration spectral set by the scaling factor. The horizontal dashed line is the 98% confidence limit on the correlation coefficient.

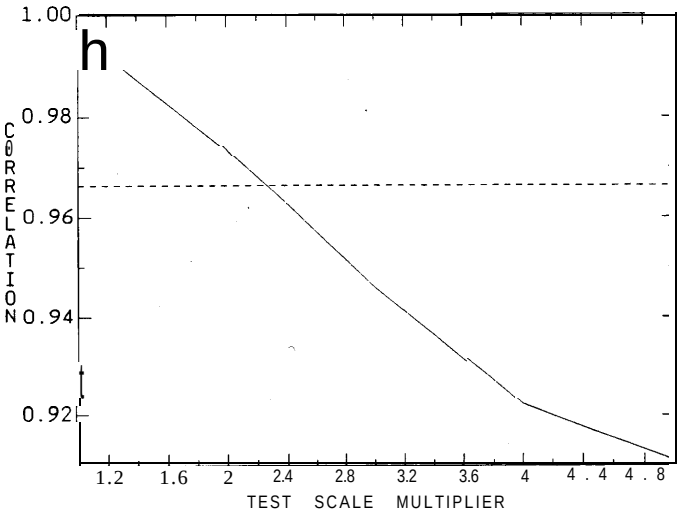

FIG. 11. The effect of the scaling factor on the correlation coefficient from the subpopulation detection algorithm as the test spectral set (the X's in Fig. 9) becomes progressively larger than the calibration spectral set by the scaling factor. The horizontal dashed line is the 98% confidence limit on the correlation coefficient.

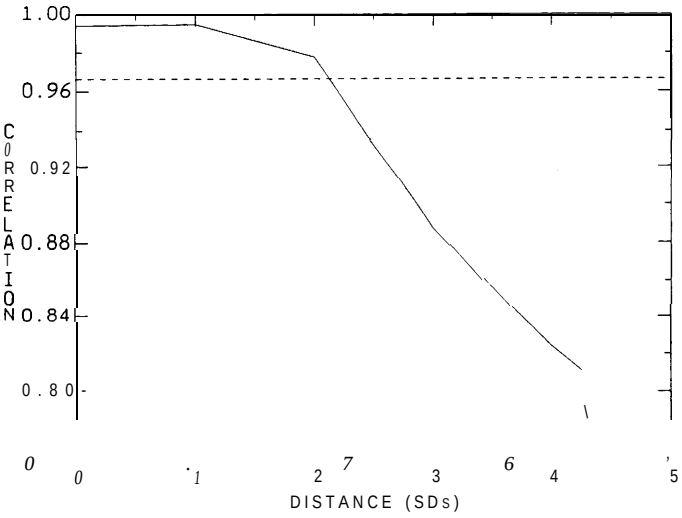

FIG. 12. The effect of location changes on the correlation between the calibration spectra and the test spectra is readily identifiable even in 128-D hyperspace. The horizontal dashed line is the 98% confidence limit on the correlation coefficient.

tribution center more closely approximated the center of the population distribution.

The effect of the location and scale of spectra on the correlation returned by the subpopulation detection algorithm is easy to visualize. Figure 9 shows a principal-component projection of the spectra from one species of wood (#1, White Ash). The squares mark the original spectra, while the X's mark the same wood spectra after the variation in the spectra is reduced at all wavelengths by a scaling factor. In Figs. 10-12, the spectra were analyzed in the full 128-D hyperspace with the subpopulation-detection algorithm. Figure 10 shows the effect of the scaling factor on the correlation coefficient from the subpopulation detection algorithm as the test spectral set becomes progressively smaller than the calibration spectral set by the scaling factor. Figure 11 shows the effect of the scaling factor on the correlation coefficient from the subpopulation detection algorithm as the test spectral set becomes progressively larger than the calibration spectral set by the scaling factor. In Figs. 10-12, the 98% confidence limit on the correlation coefficient between the calibration spectra and test spectra is shown as a horizontal dashed line (98% of the correlations are above this value when the calibration spectra and test spectra are identical in location and scale). The difference in the effect of the scaling relationship on the correlation coefficient accounts for the fact that samples 2, 18, and 23 in Fig. 8 show small distances in SDs in the columns but large distances in the rows. Figure 12 shows the effect of a location change (in effect, a change in spectral peaks) on the correlation between the calibration spectra and the test spectra. The subpopulation-detection algorithm is quite sensitive, using differences in both location and scale to differentiate among wood species spectra at the 98% level even when the spectral groups are less than 3 SDs apart.

The ARS instrument was also found to distinguish quite readily between samples oriented with the wood grain in the plane of the glass elbow, perpendicular to the elbow plane, and at an angle of 45° to the plane. This observation confirms that acoustic velocity is a major factor in the spectra because the effect of grain orientation on acoustic-wave velocity is well known.

CONCLUSION

The new acoustic-resonance spectrometer described in this paper successfully differentiates between various kinds of wood samples nondestructively. Multivariate subpopulation analysis permits results to be attained with a spectrometer that costs less than the personal computer that controls it. Acoustic-resonance spectrometry outperforms near-IR spectrometry by a wide margin in identification of the same wood species.[9]

The advantages provided by this discovery are applicable to the restoration of historical buildings, such as those of American architect Frank Lloyd Wright. The nondestructive nature of the new three-transducer interferometer ensures the on-site preservation of these national monuments.

ACKNOWLEDGMENT

This work was supported in part by the National Science Foundation through NYI award Nos. 9257998 and STI-9108764.

1. A. Abernathy, "Restoring Frank Lloyd Wright's Oak Park Home," Fine Home Building **56,** 82 (1989).
2. H. Schiffer and N. Schiffer, Woods We *Live* With (Schiffer Limited, Exton, Pennsylvania, 1977), Chap. 3.
3. H. Sakai, K. Takagi, and A. Minamisawa, Jpn. J. Appl. Phys., Supplement 27-1, 27, 55 (1988).
4. Y. Tomikawa, Y. Iwase, K. Arita, and H. Yamada, Jpn. J. Appl. Phys., Supplement 24-1, 24, 187 (1985).
5. E. Lai, B. Chan, and S. Chen, Appl. Spectrosc. 42, 526 (1988).
6. R. Lodder and G. Hieftje, Appl. Spectrosc. 42, 1500 (1988).
7. R. Lodder and G. Hieftje, Appl. Spectrosc. 42, 1512 (1988).
8. A. Mizrahi and M. Sullivan, *Calculus and Analytic Geometry* (Wadsworth Publishing Co., Belmont, California, 1986), p. 461.
9. R. Lodder and P. Nair, Appl. Spectrosc. 47, 287 (1993).